SAND81-8665
Unlimited Release
UC-62

Creep and the Corrosion Characteristics of Incoloy Alloy 800 in Molten Nitrate Salts

S. H. Goods

Prepared by Sandia Laboratories, Albuquerque, New Mexico 87115
and Livermore, California 94550 for the United States Department
of Energy under Contract DE-AC04-76DP00789.

Printed March 1981

Sandia Laboratories

Issued by Sandia National Laboratories, operated for the United States Department of Energy by Sandia Corporation.

NOTICE

SAND81-8665
Unlimited Release
Printed March 1981

CREEP AND THE CORROSION CHARACTERISTICS OF INCOLOY ALLOY 800 IN MOLTEN NITRATE SALTS

S. H. Goods
Materials Science Division 8316
Sandia National Laboratories, Livermore

ABSTRACT

The effects of deformation on the corrosion resistance of Incoloy Alloy 800 in sodium nitrate and potassium nitrate salt mixtures have been studied. Hollow tube specimens filled with the salt mixture (60%-$NaNO_3$-40% KNO_3) were tested in constant load tension creep at elevated temperatures ($550^{o} \leq T \leq 670^{o}C$). Depending on the temperature and initial stress, fracture times (and therefore salt exposure times) ranged between 300 and 1000 hours. While the fracture strain of specimens tested to failure was only slightly reduced when exposed to the salt environment, metallographic observations of polished cross-sections revealed severe surface oxidation. In order to characterize the effect of total imposed strain on oxide morphology a number of creep tests were terminated prior to fracture. Increasing deformation resulted in a more extensively damaged surface oxide as well as a more rapid rate of corrosion. EDX analysis revealed that the oxide was multiphase, with a near surface iron rich oxide above a chromium-rich oxide layer. Below $630^{o}C$ the oxide-metal interface was well defined (although irregular). Above $630^{o}C$ the interface was more diffuse with fine oxide intrusions growing into the base metal and small particles of the alloy visible in the oxide near the base metal interface.

CONTENTS

ILLUSTRATIONS

ILLUSTRATIONS
(continued)

INTRODUCTION

Incoloy Alloy 800 (I800) has been proposed for use in the receiver tube panel arrays in a number of advanced solar central receiver (SCR) concepts. Because of their high heat capacity and high thermal energy density[1], several designs require the use of molten sodium and potassium nitrate salt mixture to act as the cooling or heat transfer fluid. While there is some industrial experience with the storage, handling, and containment of these molten salts[2,3] and therefore some understanding of the behavior of alloy steels used to contain them, the information available concerns situations involving temperatures substantially below those proposed for SCR operation, that is at temperature near 600°C. It therefore becomes important to examine the corrosion compatibility of the fluid containment alloy with these nitrate based salts at temperatures more representative of the operating conditions of these facilities.

There have been a number of studies which have examined the corrosion of iron, nickel, chromium and certain alloy steels in molten salts. These tests, however, have been for the most part short term[4-7]. More recently the longer term (<1000 hr) behavior of iron based alloys has been examined[8,9]. In all of these studies however, the effects of continuous mechanical deformation on the corrosion characteristics of these alloys was not addressed. During sunlight hours, complex thermal strains will develop in the receiver tube panel due to their one sided heating by redirected sunlight (sunlight is focussed onto the receiver panel by a heliostat grid in the SCR concept). Diurnal cycling, as well as intermittent cloud cover, will result in the receiver tubes being subjected to low cycle, high strain amplitude fatigue with long hold periods at maximum temperature. At peak stress levels, the temperature will be well into the creep regime of I800. Thus, superimposed upon the fatigue cycle will be creep or plastic relaxation processes. The effects of the resulting creep fatigue interactions on the mechanical behavior and lifetime of this alloy (and other austenitic stainless steels) is a subject of much study[10,11] and will not be addressed here. Rather, a simple screening test has been devised to examine both the effects of exposure to the molten salt on the creep lifetime of I800 as well as to study the effects, if any, of continuous deformation on the structure of the oxide corrosion products formed and the adherency of these oxides to the base metal.

Corrosion may occur in one of two ways. First, if oxidation occurs via a general surface attack, a uniform surface oxide structure would be expected to form. Creep deformation (either grain boundary sliding or bulk deformation) could result in oxide cracking leading thereby to the exposure of fresh base metal. This in turn could result in an increase in oxide growth rate. This type of corrosion is generally a slow process, so in thick-

section specimens, short-time creep tests would reveal little degradation in creep rupture lifetimes or in loss of ductility. However, if corrosion occurs preferentially along grain boundaries, reduced rupture lifetime and loss of creep ductility would be expected even in relatively short-time creep tests.

EXPERIMENTAL PROCEDURE

Tensile creep tests were performed on tube stock supplied by the Pacific Tube Company. The tubing had an O.D. of 1.27 cm and a 0.29 cm wall thickness. The alloy composition is given in Table I below.

Table I
Incoloy Alloy 800 Composition (Wt.%)

Cr	Ni	Fe	C	Ti	Al	Cu	Si	Mn	S
21.15	32.81	43.35	0.04	0.47	0.52	0.52	0.21	1.02	0.002

The as-received stock solution annealed at 1050°C resulting in an ASTM grain size of 8. Optical microscopy revealed a microstructure essentially free of carbides ($M_{23}C_6$) but containing a few large ($\sim$5μm) titanium carbonitride particles.

Test specimens were fabricated from 30-cm lengths of this stock by machining a 2.54 cm long gage section (0.13 cm wall thickness) near one end of each length as shown in Figure 1. An I800 plug was then welded in the end of the specimen. The tubes were then filled with the powdered salt mixture (60 percent $NaNO_3$, 40 percent KNO_3 by weight) and mounted into a constant load tension creep frame. This specimen geometry was necessary to contain the salt when it was in a molten state since its unique surface tension properties result in its creeping out of any open container at elevated temperatures. Deformation was measured by means of a linear variable differential transformer (LVDT) attached to a high temperature extensometer cage. Temperature was maintained by using a three-zone resistance heated tube furnace controlled by a Research Incorporated furnace controller and power supply. Temperatures could be held to within 1°C of the set point throughout the duration of each test. All tests were conducted between 550 and 670°C. Scanning electron microscopy (SEM) was used to observe both fracture surfaces and surface oxide morphology. Oxide chemistry was determined by EDX, electron microprobe analysis, and X-ray analysis.

The thick wall region outside the gage section did not deform plastically. Thus, the structure of the surface oxides that form on the plastically deformed gage section could be compared to those formed on the underformed sidewalls. In addition, the exterior or air-exposed surfaces could be examined and compared to the salt-exposed inner surfaces, as shown schematically in Figure 1.

RESULTS

Creep Behavior

Figure 2 is a typical creep curve for I800 tested in the as-received condition at 600°C and at an initial stress of 317.25 MPa in air (the tube specimen was not filled with salt). For this test, the specimen was held at the test temperature for 24 hours prior to mechanical loading. Upon loading, a small amount of instantaneous plastic strain (≈0.6 percent) occurred but little or no primary creep was observed. The particular heat treatment described previously resulted in an extended teriary creep regime at all temperatures and stresses of testing. In other tests at 600°C, when the load was applied immediately upon reaching the test temperature a different type of creep behavior was observed as shown in Figure 3. Here, both the test temperature and the initial stress were the same as for the test represented by Figure 2. However, the instantaneous plastic strain was much greater (≈6.5 percent) than that induced in the specimens annealed prior to testing. The primary creep region was also greatly exaggerated compared to the test shown in Figure 2 with the creep rate decreasing rapidly after several hours.*

This difference in initial creep behavior between the two tests shown can be attributed to the effect of temperature on the carbide microstructure. At 600°C $M_{23}C_6$ carbides form after several hours. Thus, the 24-hour hold at the test temperature prior to mechanical loading for the specimen shown in Figure 2 represents a grain boundary carbide forming and stabilizing heat treatment. The evolution of the carbide strengthened microstructure is shown in Figure 4 and correlates quite closely with the creep behavior shown in Figure 3. The carbides begin to decorate the grain boundaries heavily after about 8 hours at temperature (Figure 4c) corresponding to time when the creep rate begins to rapidly decrease. The carbides that form resulted in a microstructure that is strengthened against plastic deformation. For the specimen shown in Figure 3, this strengthening microstructure did not form prior to loading, thereby resulting in a greater initial offset. As the carbides precipitate, the specimen becomes more resistant to deformation and the creep rate falls off dramatically.

The apparent strengthening attributed to the carbide microstructure can be the result of the high stress sensitivity of the alloy at these temperatures and fine grain size. Because of the fine grain size, the precipitate-free grain boundaries are free to slide. As precipitation occurs the grain boundaries are increasingly pinned and can support shear stresses. The resulting decrease in grain boundary sliding and stress in the matrix can result in a greatly reduced creep rate.

*That the test shown in Figure 3 was conducted as a salt-filled specimen, while the specimen represented by Figure 2 was unfilled should have little bearing on the initial creep behavior. Thus, the comparison drawn between these two tests at the same temperature and initial stress remain valid.

While the salt exposed creep specimen exhibited a shorter creep-rupture lifetime than the air-exposed specimen, the difference is more likely the result of test to test variation rather than to any large environmental effect. Figure 5 compares the effect of salt and air exposure on the creep behavior of the alloy at 630°C and at an initial stress of 275.85 MPa. The longer life of the test in salt is opposite to the results at 675°C. Comparisons at other temperatures show no clear trend with regard to salt induced degradation of the mechanical properties of I800. Observation of the fracture surfaces of all specimens tested revealed mixed mode failure with regions of transgranular fracture adjacent to intergranular fracture. The presence of salt within the tube during testing did not significantly influence the fracture surface morphology in these creep tests.

Oxide Structure

While mechanical testing alone did not reveal the presence of environmental attack, metallographic observation of the salt-exposed tensile specimens clearly demonstrated salt induced corrosion. Figure 6a is a scanning electron micrograph of a salt exposed tube sidewall. The section shown is from a deformed gage section of a creep specimen tested at 550°C. For this specimen, the test was terminated prior to fracture after approximately one percent creep strain. The oxide is the darker region near the center of the micrograph. Above the oxide is a protective nickel plate which was applied after creep testing and sectioning in order to protect the surface scale during metallographic preparation. Below the oxide layers is the base alloy. The lighter and darker regions within the oxide scale indicate that it is multiphase. EDX analysis (Figure 6b-d) was used in a qualitative way to map the iron, chromium and nickel concentrations in the oxide phases and base material. The spot density patterns shown reveal that the near surface oxide phase was iron-rich and chromium and nickel poor. Chromium concentration in the molten salt is known to increase with exposure time[9]. Thus the lack of chromium in the near surface oxide can be explained as the dissolution of Cr into the melt at the salt-metal interface. The concentration of nickel in solution however does not increase with exposure time. The absence of nickel in the near surface layer suggests that the surface oxide forms as the result of iron diffusion to, and its subsequent oxidation at, the salt-metal interface. The underlayer oxide was noticeably depleted in iron while chromium and nickel are present in concentrations roughly equal to that found in the base alloy.

At higher exposure temperatures, salt induced corrosion continued at a relatively rapid rate. Figure 7a shows that at 570°C a 20μm oxide scale was formed in 750 hrs. of exposure to the molten nitrate salt mixture. As in the previous figure, the creep test was terminated after one percent strain. The oxide was again multiphase with the surface oxide being iron rich and depleted in chromium and nickel. At this higher temperature however, the subsurface oxide was slightly enriched in chromium. The large blocky feature near the bottom of the micrograph is a titanium carbonitride particle (revealed as being depleted in all the major alloying constituents). As the temperatures of testing was increased, the subsurface oxide became increasingly enriched in chromium. Figure 8a is a scanning electron micrograph of the surface of an undeformed tube sidewall exposed to the salt mixture at 670°C for 443 hours. This specimen was not nickel plated and the flaring and very bright features are aftifacts induced by the polishing procedure.

Figure 8b shows that the surface oxide formed was iron rich while the subsurface oxide was depleted in Fe. Beneath this surface layer was an oxide which was chromium rich and iron poor. The chromium analysis in Figure 8c revealed a third region within the oxide nearest the oxide-metal interface which was depleted in Cr.

Figure 9c shows the results of an electron microprobe analysis performed on the sidewall pictured in Figure 8a. The oxide-metal interface is shown as the dashed vertical line corresponding to the observation of oxygen in the specimen. While only semi-quantitative (especially for light elements like oxygen), these results confirm the presence of the different phases and their positions relative to each other as described above. The near-surface layer is clearly an iron oxide essentially free of chromium. As also shown in Figure 8b, the microprobe analysis revealed the chromium-rich subsurface layer to be iron-poor. This depletion is not nearly so great, however, as in the depletion of Cr in the surface layer. Nearest the oxide base metal interface the microprobe analysis also revealed the chromium depleted layer forming only at the highest temperatures (650-670°C) studied. The oxide structure formed at these temperatures on I800 are similar to those formed on 304 stainless steel tubing at 600°C after over 8000 hours exposure[8].

X-ray analysis using the Debye-Scherrer technique indicated the presence of α-Fe_2O_3, γ-Fe_2O_3 as well as a phase which might be $Fe(FeCr)_2O_4$ spinel. The similarity of the $Fe(FeCr)_2O_4$ pattern to the pattern formed by Fe_3O_4 made positive identification of the spinel phase difficult. It is possible that at these elevated temperatures increased chromium mobility resulted in a spinel phase which was higher in Cr content than that formed at lower temperatures. This redistribution of chromium into the spinel phase can explain the observed Cr enhanced mid-layer in the oxide while also accounting for the depletion in chromium in the region adjacent to it.

Figures 6a and 7a are micrographs of surface oxides formed on tube sidewalls which were continuously deforming during exposure to molten salt. In both cases, the total creep strain imposed during the tests was approximately one percent. These low strains had little effect on either oxide structure or the rate of corrosion when compared to nondeformed tube sidewalls exposed to the salt mixture under the same conditions. Increased levels of deformation did affect oxide morphology significantly. Figure 10 shows the surface condition of three different regions of a specimen creep tested at 650°C for 550 hours to a total creep strain of 10 percent. In Figure 10c the air exposed or exterior sidewall of the specimen shows no observable oxidation. Exposure to the undeformed sidewall surface to the molten salt resulted in a uniform and adherent oxide approximately 10μm thick (Figure 10b). The oxide formed on the salt exposed gage section (Figure 10a) exhibited a much thicker oxide (20-25μm). The oxide can be seen to penetrate down grain boundary cracks formed during deformation.

Additionally, the oxide itself was porous and cracked, unlike the oxide formed on the undeformed surface. It can be seen that the cracking in the oxide corresponds to the presence of subsurface grain boundary cracks. Increasing the imposed strain resulted in an oxide which was more extensively damaged, as shown in Figure 11a. The oxide shown in this figure formed on the sidewall of a tube deformed to a total creep strain of 24 percent in 443 hours at 670°C. The oxide was more extensively cracked than that shown in the

Figure 10a. The oxide on the deformed surface was, as in the previous figure, thicker than that formed on the undeformed surface (Figure 11b).

The structure of the oxide-base metal interface also depends on the exposure temperature. At the lowest temperature the interface, while irregular, was well defined as is shown in Figure 6a. At the highest temperatures (650-670°C), the interface was more diffuse as shown in Figures 8a and 10b. At these high temperatures the interface formed on the undeformed sidewalls can be characterized by the fine fingerlike growth of the oxide into the alloy. It should be noted that the spacing of these fine intrusions into the alloy was much smaller than the specimen grain size. The observed structure is therefore not caused by grain boundary attack. In Figures 10a and 11a, the oxides formed on the deformed sidewalls contain small isolated fragments of base metal near the interface. The difference in the structure of the interface between the undeformed and deformed sections is particularly clear in Figure 11 and may be the result of the continuous creep strain deforming and fracturing fine structure of the undisturbed oxide interface.

CONCLUSIONS

The results of this work indicate that in the high temperature region of the SCR tube panel (near 600°C) I800 tubing in the solution annealed condition is microstructurally unstable. $M_{23}C_6$ carbide precipitate rapidly along grain boundaries resulting in an increased resistance to grain boundary sliding. The high stress sensitivity of the alloy at these temperatures along with the ability of the pinned grain boundaries to support the mechanical load can explain the decrease in creep rate as the precipitation phenomenon occurs. While these microstructural instabilities do not preclude the use of the alloy in receiver tube application, stabilizing heat treatments may be necessary, especially considering the cyclic nature of thermal and mechanical loading of the system.

The results of the mechanical testing alone did not reveal a degredation in structural properties. Deformation did not change the mode of corrosive attack. The observed grain boundary penetration was the result of deformation induced grain boundary cracking exposing fresh base metals to the molten salt. At low levels of strain, deformation had little effect on oxide morphology or growth kinetics. At higher strains (approximately 10 percent and greater) the oxides formed on the deformed surfaces were cracked and more porous than those formed on undeformed sidewalls. The oxide cracking caused by the imposed creep strain resulted in the exposure of fresh base metal to the molten salt with the net effect being an acceleration of the overall corrosion rate. In addition at high temperature, deformation altered the fine structure of the oxide metal interface which may also affect the growth rate of the surface scale.

Exposure temperatures is an important variable in the structure and chemistry of the oxide which form. At the lower temperatures of this study the oxide was multiphase with a surface layer rich in iron. X-ray analysis indicates the presence of both α-Fe_2O_3 and γ-Fe_2O_3. The subsurface oxide containing both iron and chromium is possibly an $Fe(FeCr)_2O_4$ spinel phase. At higher temperatures this subsurface oxide became increasingly rich in chromium while the region nearest the base metal interface was depleted in Cr.

The structure of the oxide-metal interface itself was sensitive to temperature. At the lower exposure temperatures the interface was irregular but sharply defined. At higher temperature the interface was more diffuse, consisting of fine intrusions of oxide into the base metal and in deformed surfaces, of isolated fragments of alloy in the oxide near the interface.

The high alloy content of Incoloy Alloy 800 does not guarantee resistance to corrosion in molten nitrate salt environments. The formation of oxide scales, often in excess of 15μm in these relatively short exposure times, indicate the potential for severe surface corrosion in the context of long term service application.

In summary, the results of the experiment program reveal that:

1. The salt environment did not significantly affect the high temperature mechanical properties of I800 in the short term tests performed.

2. Incoloy Alloy 800 is subject to oxidation in molten nitrate salts at temperatures representative of receiver tube panel operation.

3. The oxides which form are multiphase and occur as the result of a general surface attack.

4. The rate of oxidation may be significant in determining ultimate lifetime of salt cooled receiver panels.

REFERENCES

1. K. W. Battelson, et al, 1980 Solar Central Receiver Technology Review, SAND80-8235, Sandia National Laboratories, Livermore, CA.

2. "Molten Salt Safety Study Final Report", MCR-80-1305, Martin Marietta Co., (1980).

3. A. P. Vosnick and U. W. Uhl, Chem. Engr., May 29, 1963, p. 129.

4. A. P. Arvia, J. J. Podesta and R. C. V. Piatti, Electrochem. Acta., 1972, Vol. 17, p. 33.

5. I. D. Dirmeik, Corrosion NACE, 1969, Vol. 25, $4, p. 180.

6. S. L. Marchiano and A. J. Arvia, Electrochem. Acta, 1972, Vol. 17, p. 861.

7. A. Baraka, A. I. Abdel-Rohman, and A. A. El Hosary, Br. Corres. J., 1976, Vol. 11, No. 1, p. 44.

8. C. M. Kramer, W. H. Smyrl and W. B. Estill, J. Matl. for E. Systems, 1980, Vol. 1, p. 59.

9. R. W. Bradshaw, SAND80-8856, Sandia National Laboratories, Livermore, CA, 1980.

10. S. Majumdar, "Biaxial Creep-Fatigue Behavior of Type 316H Stainless Steel Tube", ANL-79-33, Argonne National Labs,, 1979.

11. S. Majumdar, "Biaxial Creep-Fatigue Behavior of Materials for Solar Thermal Systems", ANL-80-34, Argonne National Labs., 1980.

ACKNOWLEDGEMENTS

The author wishes to acknowledge the technical assistance of T. J. Sage for his help in all aspects of the experimental program. C. W. Karfs and D. R. Boehme are acknowledged for their assistance in scanning electron microscopy and x-ray diffraction identification, respectively.

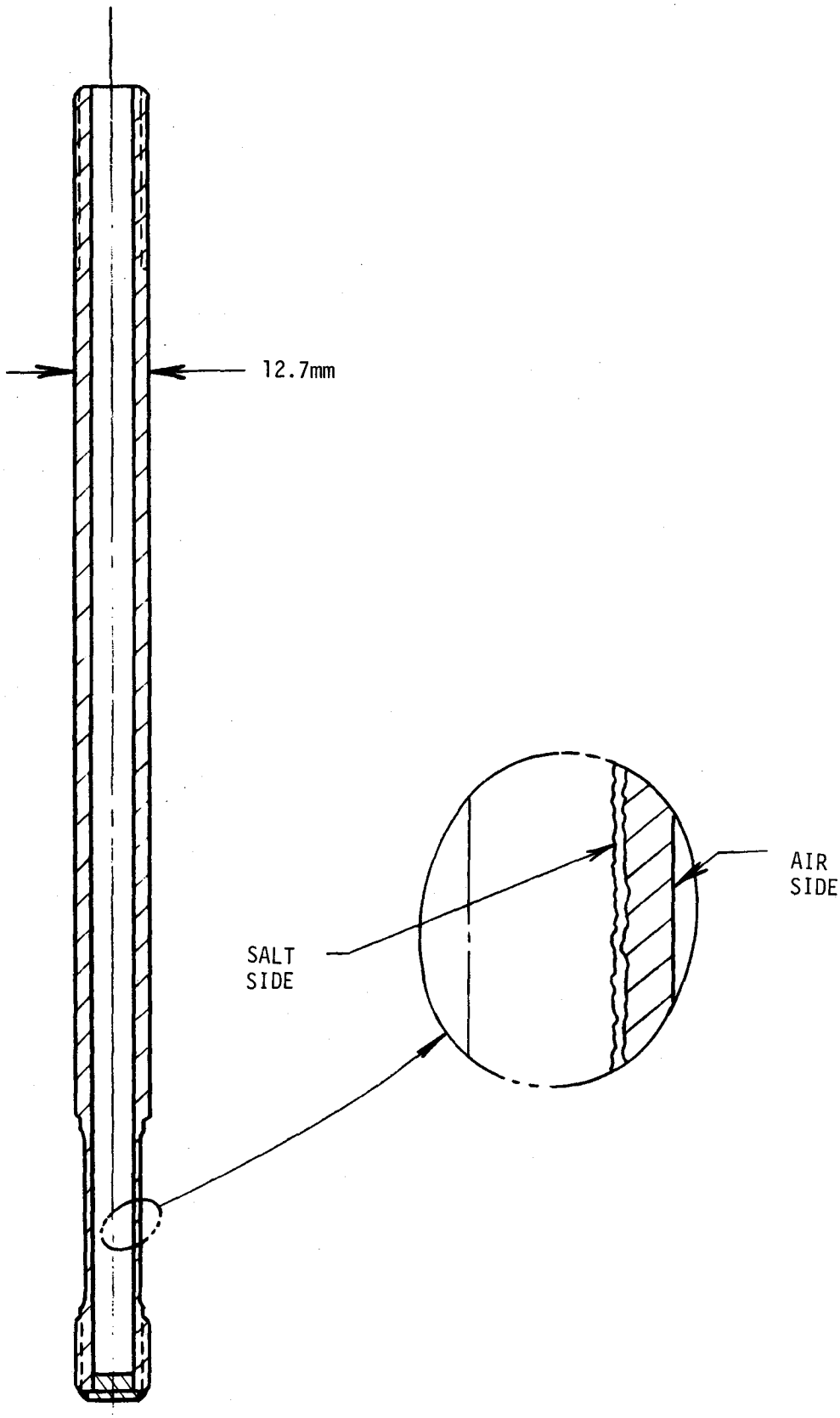

Figure 1. Creep specimen. The molten salt was contained within the hollow tube by an I800 plug welded into the bottom end. The long length of tubing above the gage section exited through the top of the furnace chamber. The resulting temperature gradient aided in containing the salt. Exposure to the salt resulted in the formation of an inner wall oxide scale at all temperatures of testing.

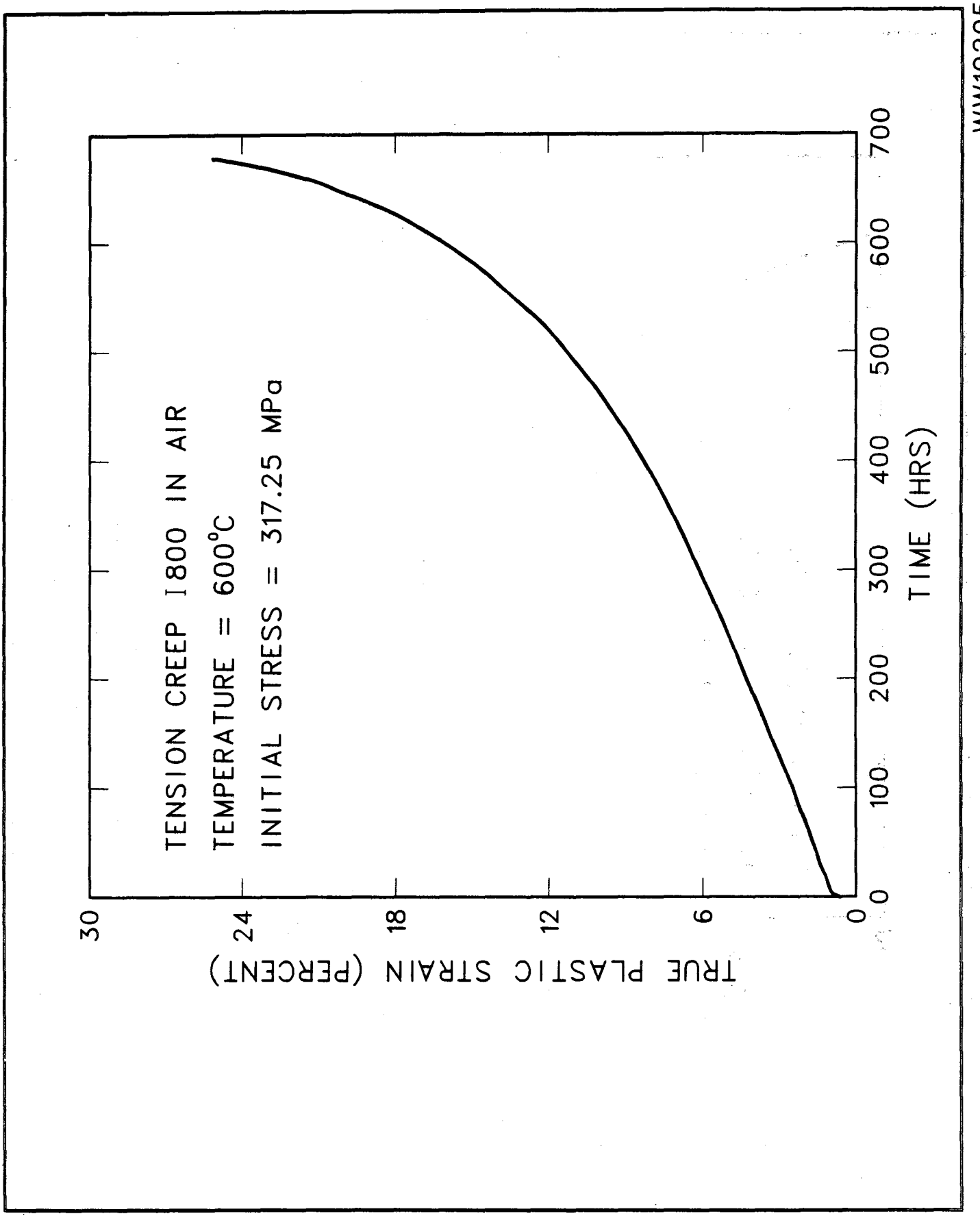

Figure 2. Constant load creep curve for Alloy 800 tested at 600°C and at an initial stress of 317.25 MPa. Prior to mechanical loading the specimen was brought to and held for 24 hours at the test temperature.

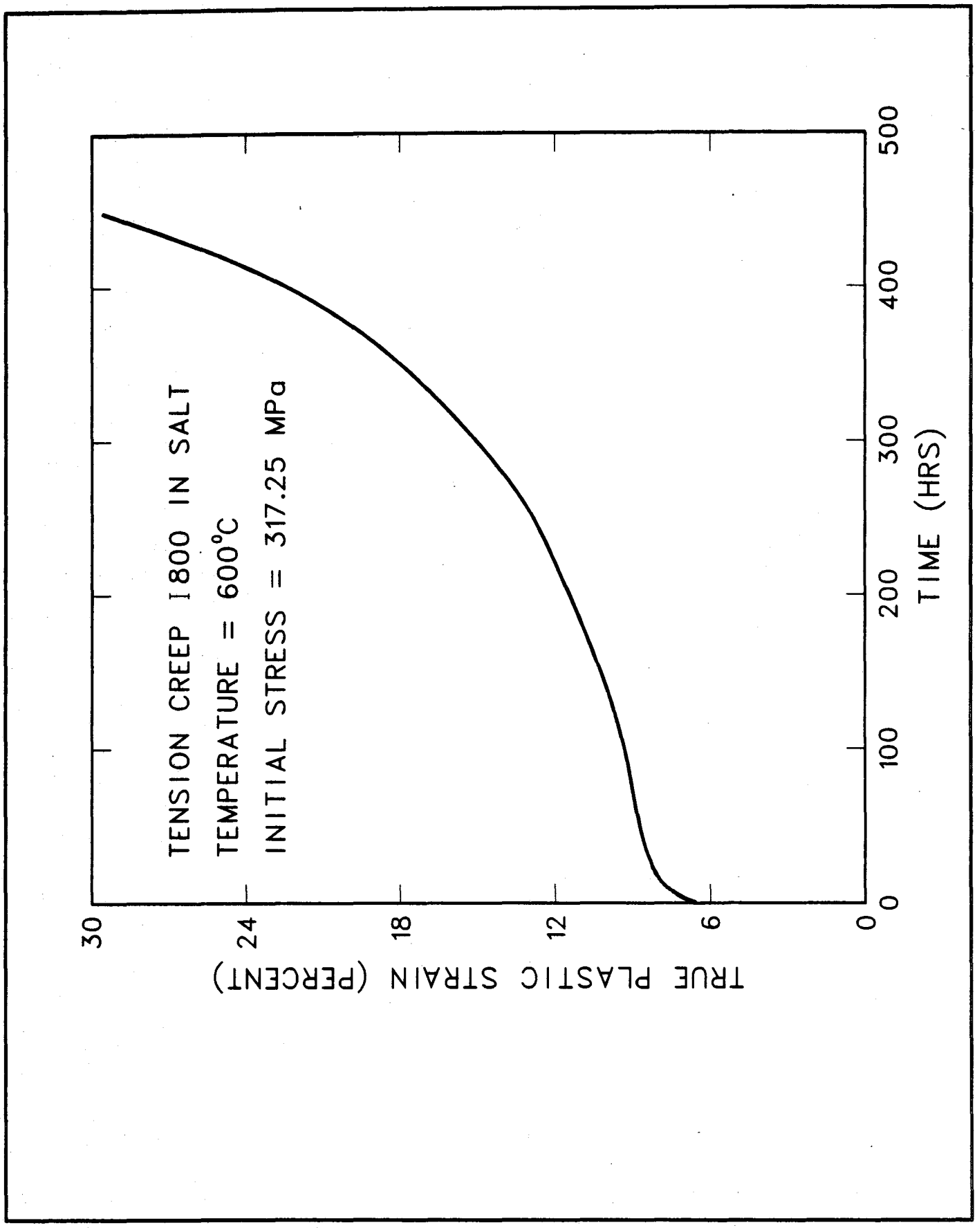

Figure 3. Constant load creep curve for a salt exposed I800 specimen tested at 600°C and at an initial stress of 317.25 MPa. The specimen was mechanically loaded immediately upon reaching the test temperature.

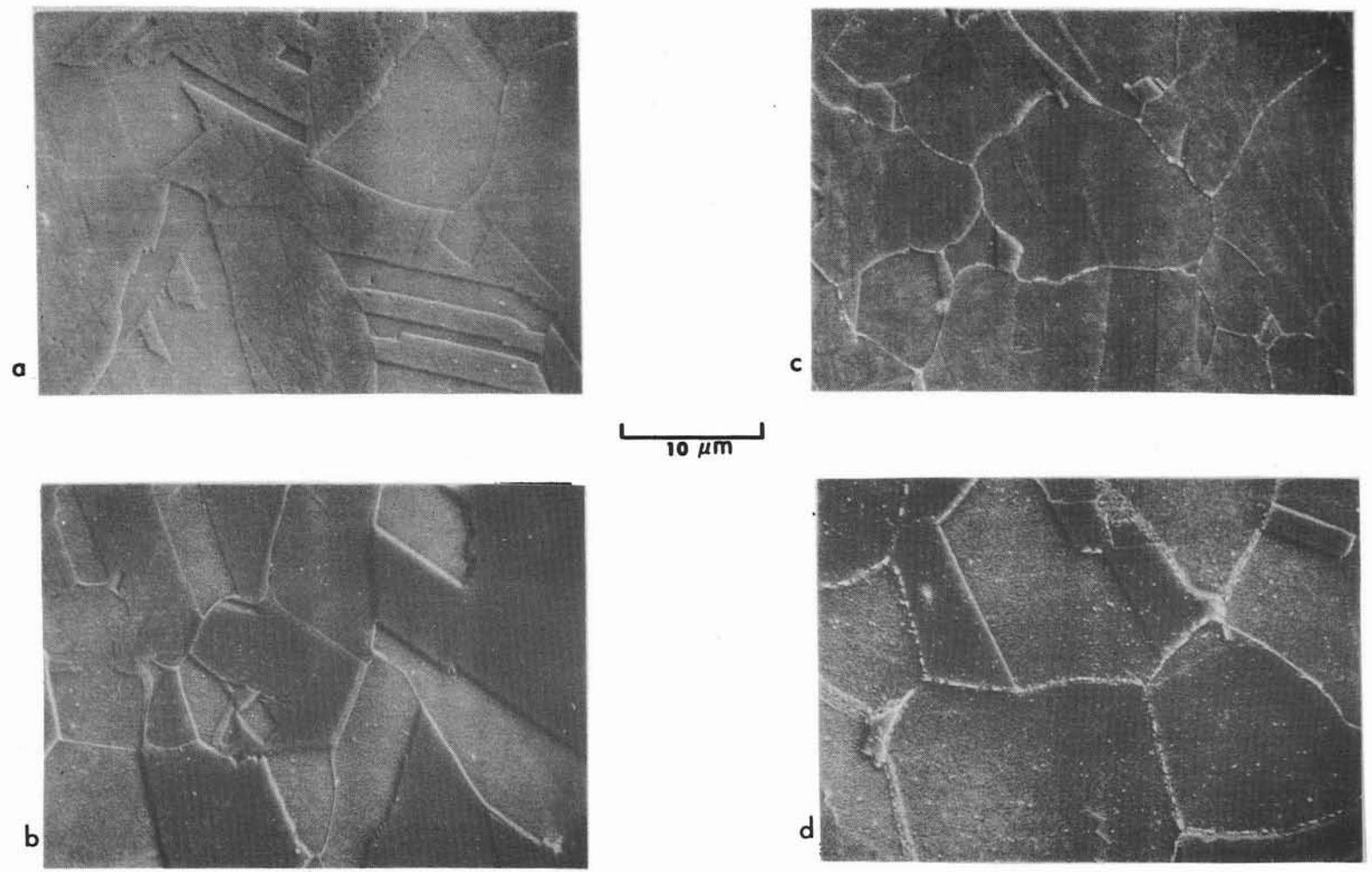

Figure 4. Scanning electron micrographs of polished and etched cross-sections of I800 tubing showing the evolution of the microstructure for different annealing times at 600°C. For Figure 4a - annealing time, 1 hour, Figure 4b - 5 hours, Figure 4c - 8 hours, Figure 4d, 12 hours.

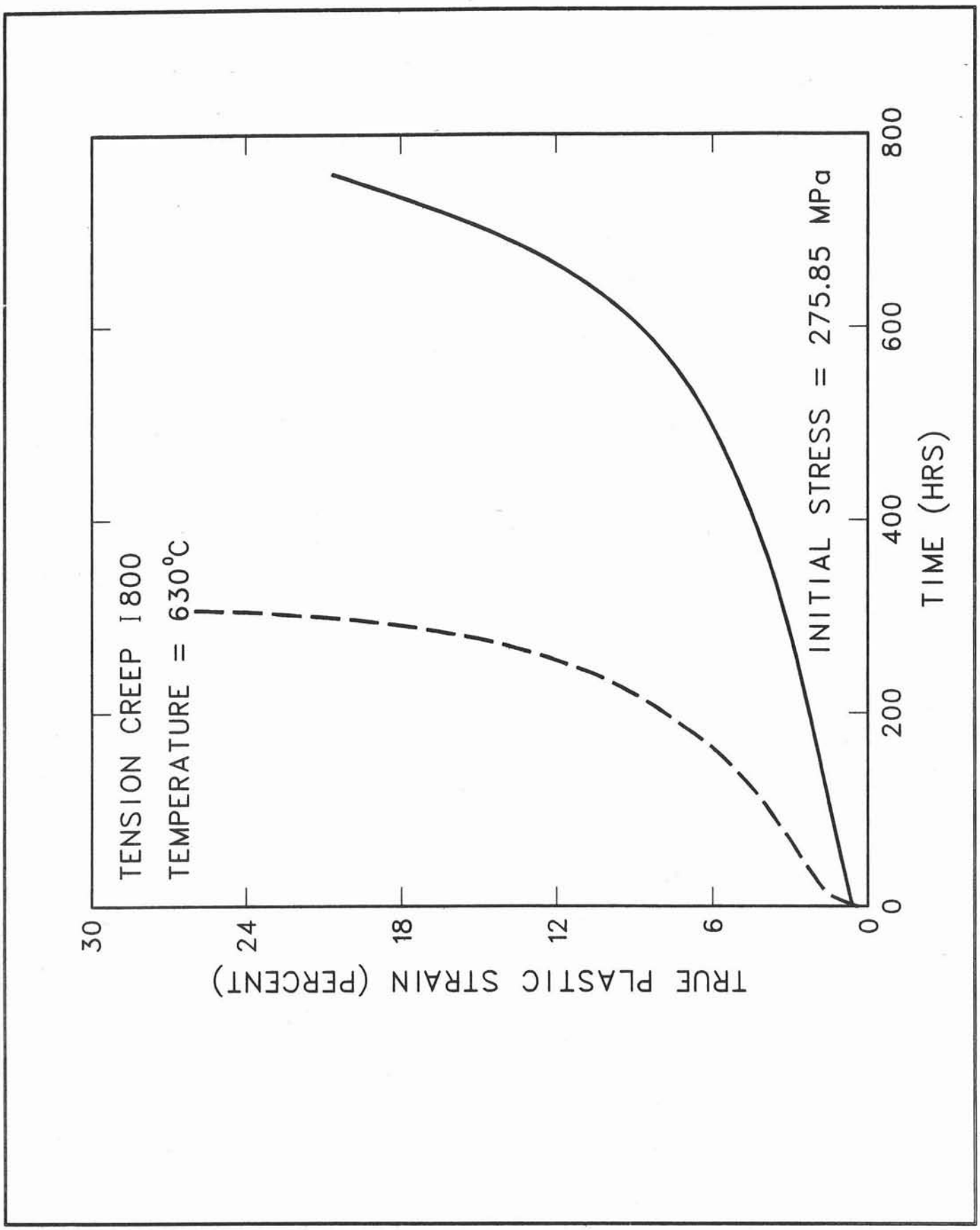

Figure 5. Constant load creep curves for I800 at 630°C and at an initial stress of 275.85 MPa tested in salt (———) and in air (-----).

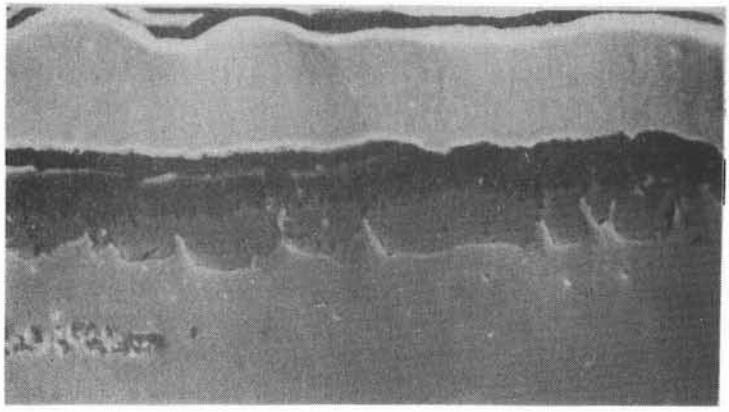

SALT EXPOSED SIDEWALL
DEFORMED
550C, 1000 HR.

a. 20 μm

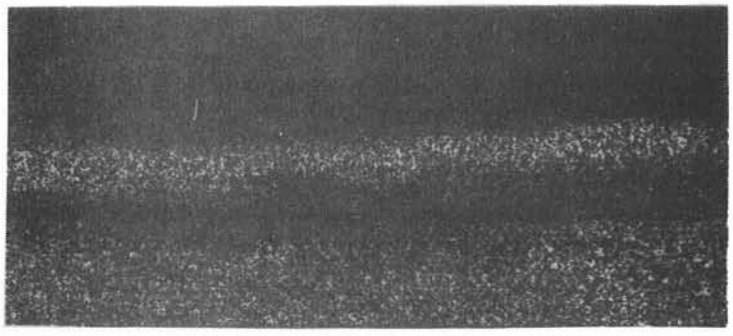

IRON

b.

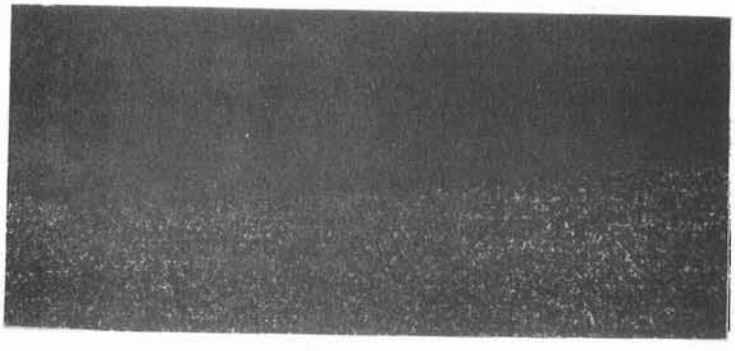

CHROMIUM

c.

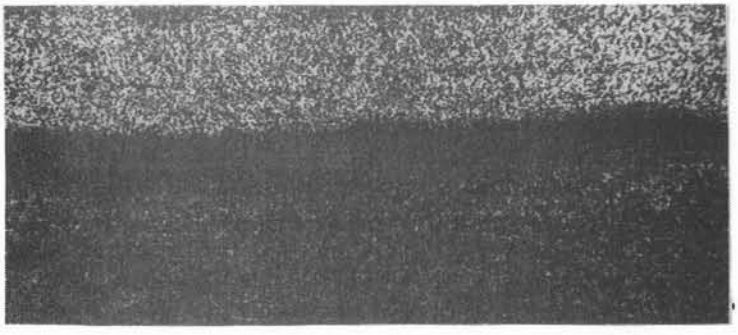

NICKEL

d.

Figure 6. Figure 6a. Scanning electron micrograph of salt exposed and deformed inner sidewall. The test was conducted at 550°C for 1000 hours and terminated after approximately 1% strain. The material above the oxide is a nickel plate applied to protect the surface during polishing. Figures 6b-3. EDX patterns showing the relative distribution of the principle alloying elements in the oxide and base metal for the section shown in Figure 6a.

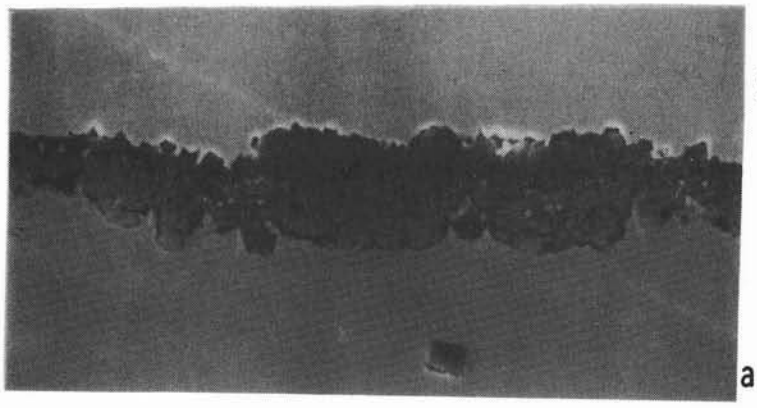

SALT EXPOSED SIDEWALL
DEFORMED
570 C, 750 HR.

a.

20 μm

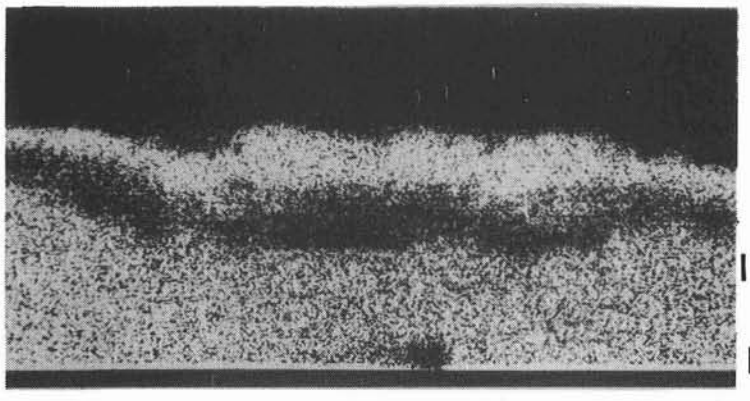

IRON

b.

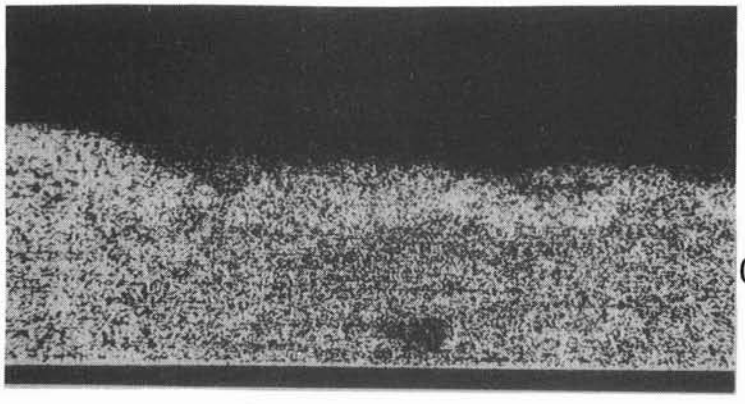

CHROMIUM

c.

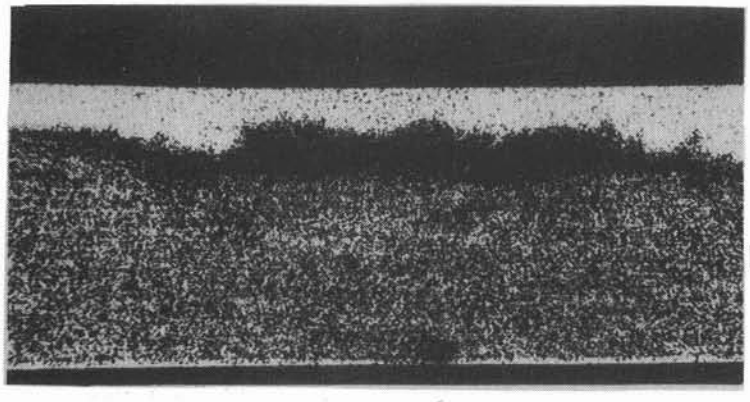

NICKEL

d.

Figure 7. Figure 7a. SEM of salt exposed and deformed inner sidewall. The test was conducted at 570°C for 750 hours and terminated after approximately 1% strain. Figure 7b-d. EDX patterns showing the relative distribution of the principle alloying elements in the oxide and base metal shown in Figure 7a.

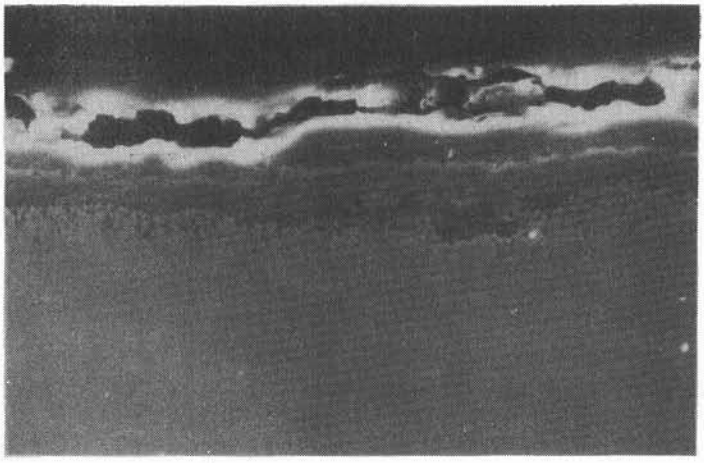

SALT EXPOSED SIDEWALL
UNDEFORMED
670 C, 443 HR.

a.

20 μm

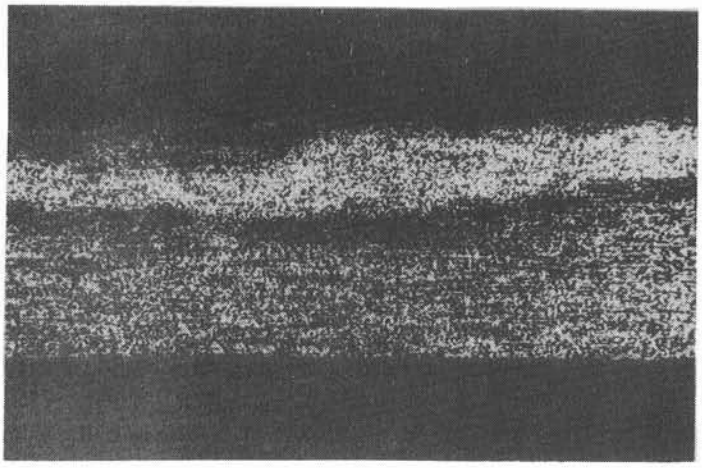

IRON

b.

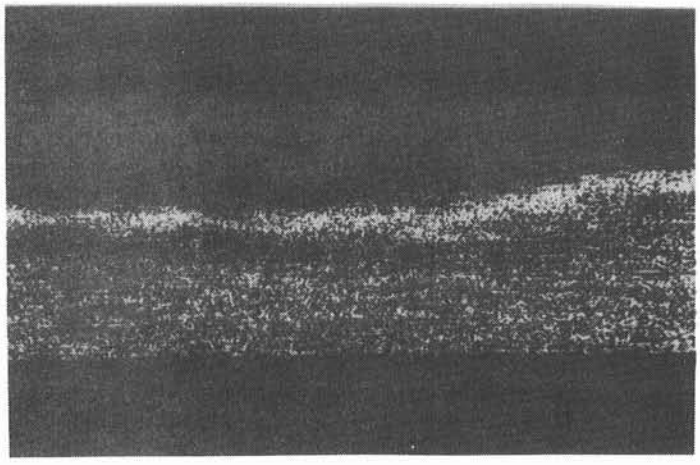

CHROMIUM

c.

Figure 8. Figure 8a. SEM of salt exposed undeformed sidewall (670°C). The flaring and irregular features above the oxide are an artifact of the metallographic preparation and not part of the microstructure. Figure 8b and 8c. EDX analysis showing the distribution of iron and chromium in the oxide and base metal.

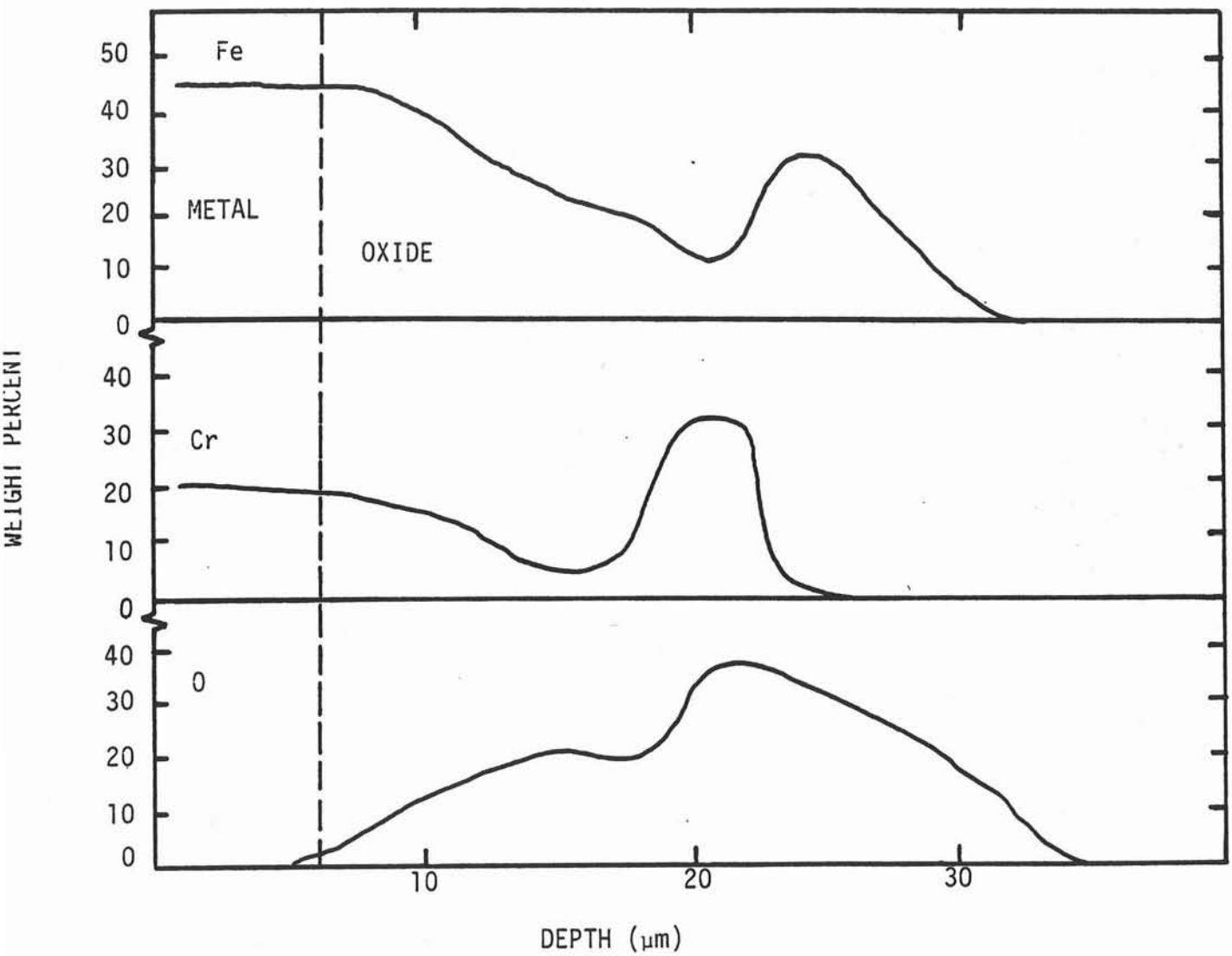

Figure 9. Electron microprobe analysis of the specimen shown in Figure 8a. The results illustrate the Cr depleted region nearest the oxide-metal interface above which is a Cr rich oxide. The near-surface oxide is Cr free and is composed of only iron oxide.

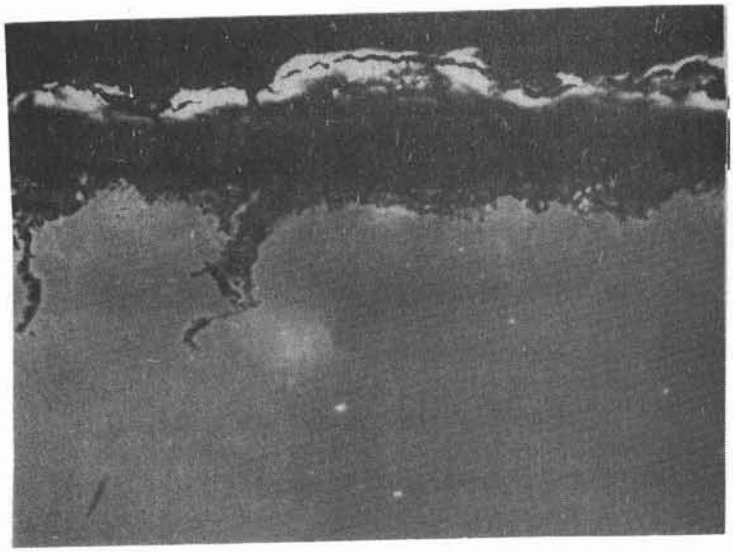

SALT EXPOSED SIDEWALL
10 % STRAIN
650 C, 550 HR.

a.

20 μm

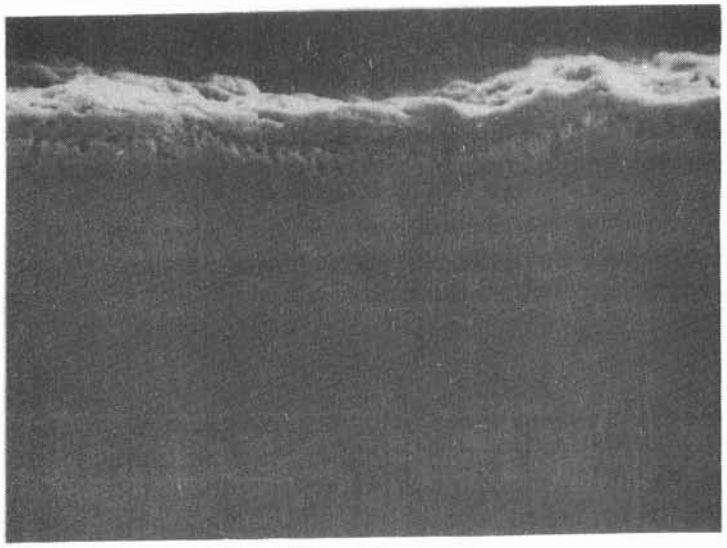

SALT EXPOSED SIDEWALL
UNDEFORMED

b.

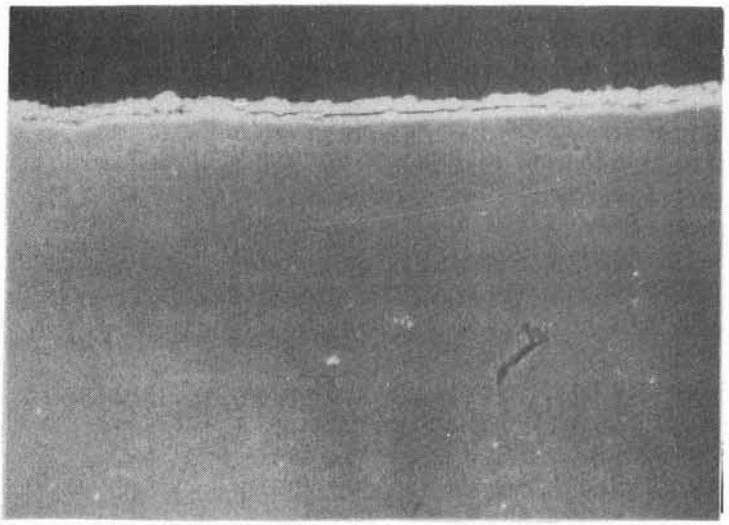

AIR EXPOSED SIDEWALL
UNDEFORMED

c.

Figure 10. Surface oxide structure formed during exposure to molten nitrate salt (SEM). Figure 10a. Oxide structure formed on salt exposed gage surface (deformed inner tube wall). Figure 10b. Oxide structure formed on salt exposed, non-deforming sidewall. Figure 10c. Air exposed sidewall. Deformation results in a thicker, more porous oxide.

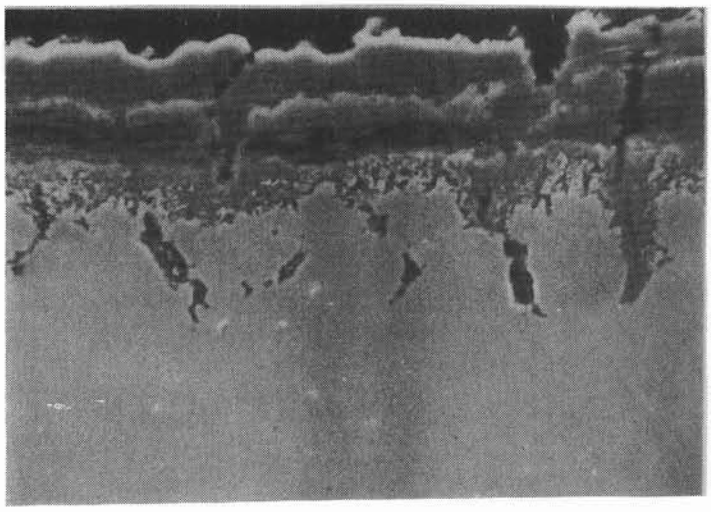

SALT EXPOSED SIDEWALL
24 % STRAIN
670 C, 443 HR.

a.

20 μm

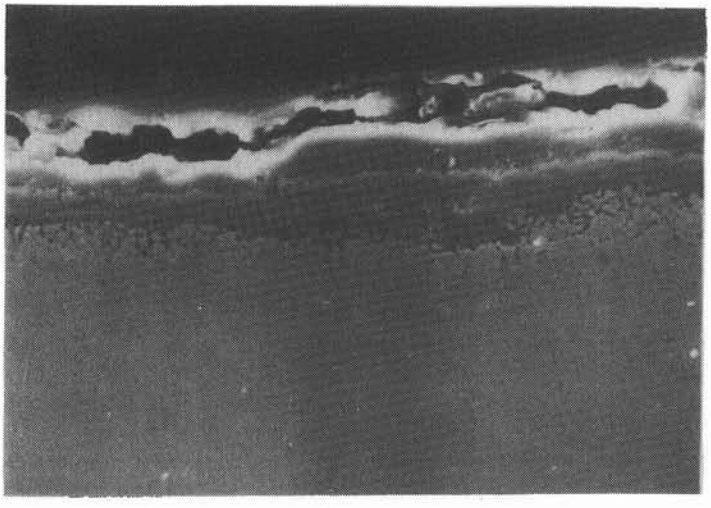

SALT EXPOSED SIDEWALL
UNDEFORMED

b.

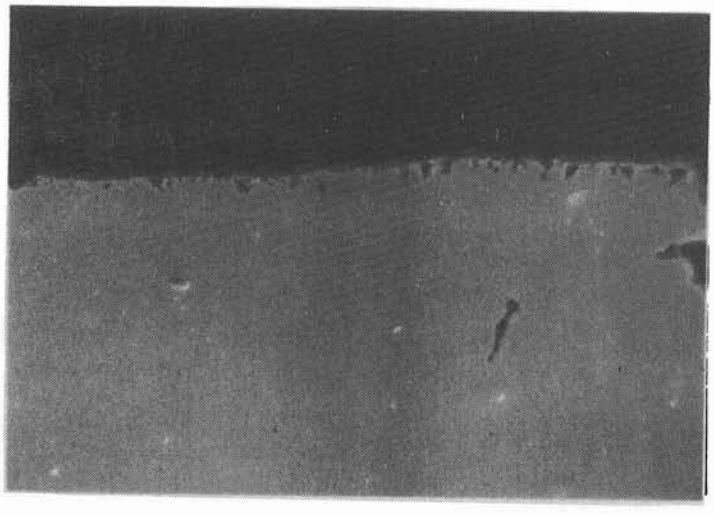

AIR EXPOSED SIDEWALL
DEFORMED

c.

Figure 11. Surface oxide structure formed during exposure to molten nitrate salt (SEM). Figure 11a. Oxide structure on salt exposed gage surface. Figure 11b. Oxide structure formed on non-deforming sidewall. Figure 11c. Air exposed sidewall. As deformation increases so does the degree of damage in the oxide.

UNLIMITED RELEASE

INITIAL DISTRIBUTION:

USDOE (4)
Division of Thermal and Mechanical Energy Storage Systems
MS 6B025 Room 1G-100
Forrestal Building
Washington, D.C. 20585
Attn: J. H. Swisher
J. Gahimer
M. Gurevich
J. Brogan

USDOE
Albuquerque Operations Office
Special Programs Division
P.O. Box 5400
Albuquerque, NM 87115
Attn: D. Schueler

USDOE (2)
San Francisco Operations Office
1333 Broadway
Oakland, CA 94612
Attn: D. Elliott
L. Prince

USDOE (4)
Division of Solar Thermal Energy Systems
600 E. Street N.W.
Room 419
Washington, D.C. 20585
Attn: G. W. Braun
M. U. Gutstein
J. E. Rannels
W. Auer
K. Cherian

Aerospace Corporation (2)
2350 El Segundo Blvd.
El Segundo, CA 90009
Attn: P. Mathur
L. R. Sitney

William D. Beverly
Boeing Engineering and Construction Co.
P.O. Box 3707
Seattle, WA 98124

Dr. C. A. Bolthrunis
Badger Energy, Inc.
One Broadway
Cambridge, MA 02142

William F. Clancy
Babcock and Wilcox Company
P.O. Box 351
Barberton, OH 44203

J. H. DeVan
Oak Ridge National Laboratory
Box X
Oak Ridge, TN 37830

James Elsner
General Electric
1 River Road
Schenectady, NY 12345

EPRI (2)
P.O. Box 10412
3412 Hillview Avenue
Palo Alto, CA 94303
Attn: J. Bigger
T. R. Schneider

Donald C. Erickson
627 Ridgely
Annapolis, MD 21401

Dr. R. W. Foreman
Part Chemical Company
8074 Military Avenue
Detroit, MI 48204

General Atomic Co. (2)
P.O. Box 81608
San Diego, CA 92138
Attn: Thomas H. Van Hagan
Daniel L. Vrable

Skip Gross
MSA Research
Evans City, PA 16033

Steve PL Harnden
Airzona Public Service Company
P.O. Box 21666
Phoenix, AZ 85036

JPL (4)
4800 Oak Grove Drive
Pasadena, CA 91103
Attn: V. Truscello
R. Manvi
J. Becker
W. Phillips

John Neill
Advanced Energy Concepts
11722 Sorrento Valley Rd.
Suite I
San Diego, CA 92121

Soeren S. Nielsen
Gould, Inc.
40 Gould Center
Rolling Meadows, IL 60008

Bill Oberjohn
Babcock and Wilcox
Box 835
Alliance, OH 44601

Olin Corporation (3)
275 Winchester Ave.
New Haven, CT 06511
Attn: Louis C. Fiorucci
Stephen L. Goldstein
Joe K. Mensah

Olin Corporation (3)
120 Long Ridge Road
Stamford, CT 06904
Attn: Norman Christopher
Gerald A. Haib
Robert E. Smith

Dr. Robert A. Osteryoung
Department of Chemistry
State University of New York at Buffalo
Buffalo, NY 14214

Prof. Harald A. Oye
Institutt for uorganisk kjemi
Norges tekniske hogskole
Universitetet i Trondheim
N7034 Trondheim - NTH, Norway

Pacific Gas and Electric (3)
3400 Crow Canyon Road
San Ramon, CA 94583
Attn: Helena T. Rowland
Harold E. Seielstand
Jay Raggio

Rockwell International
8900 De Soto Avenue
Canoga Park, CA 91304
Attn: Anarg Z. Frangos

Rockwell International/ESG
8900 De Soto Avenue
Canoga Park, CA 91304
Attn: Ted Johnson

Rockwell International/ETEC (2)
8900 De Soto Ave.
Canoga Park, CA 91304
Attn: Rick L. Howerton
Jerry B. Brukiewa

George H. Rowe
Combustion Engineering
1000 Prospect Hill Road
Windsor, CT 06095

SERI (8)
1536 Cole Blvd.
Golden, CO 80401
Attn: B. Butler
K. Touryan
B. P. Gupta
C. Wyman
P. A. Roberts
P. Russell
R. G. Nix
R. Ortiz (SERI Library)

Stuart A. Shiels
Westinghouse Electric Corporate
Advanced Reactors Division
Box 158
Madison, PA 15663

Richard D. Smith
Rocket Research Company
York Center
Redmond, WA 98052

Alan Snelson
ITT Research Institute
10 W 35 Street
Chicago, IL 60616

Donald J. Spellman
Gas Cooled Reactor Assoc.
3344 No. Torrey Pines Road
La Jolla, CA 92137

Pierre Spiteri
EDF
Les Renaidierz
Ecuelles
France

United Engineers and Construction
30 S. 17th Street
Philadelphia, PA 19103
Attn: John B. Mulligan

Robert J. Walter
Rocketdyne
6633 Canoga Ave.
Canoga Park, CA 91360

Sydney H. White
EIC Labs., Inc.
55 Chapel Street
Newton, MA 02158

Fred F. Witt
General Electric
3172 Porter Drive
Palo Alto, CA 94304

George Yenetchi
Solar Thermal Systems
Division of Exxon Enterprises Inc.
P.O. Box 592
Florham Park, NJ 07932

C. Winter, 4000
A. Narath, 4000
J. H. Scott, 4700
G. E. Brandvold, 4710; Attn: B. W. Marshall, 4713
R. P. Stromberg, 4714
V. L. Dugan, 4720; Attn: J. V. Otts, 4721
J. F. Banas, 4722
J. A. Leonard, 4725
J. K. Galt, 5000
R. S. Claassen, 5800
R. G. Kepler, 5810
M. J. Davis, 8530; Attn: R. W. Rohde, 5832
N. J. Magnani, 5840; Attn: D. W. Schaefer, 5841
T. B. Cook, 8000
W. E. Alzheimer, 8120; Attn: R. J. Gallagher, 8124
A. N. Blackwell, 8200
B. F. Murphey, 8300
D. M. Schuster, 8310
R. W. Mar, 8313
R. W. Bradshaw, 8313
A. S. Nagelberg, 8313
D. A. Nissen, 8313
J. C. Swearengen, 8316
S. H. Goods, 8316 (25)

R. L. Rinne, 8320
M. E. Stoll, 8341
L. Gutierrez, 8400
R. A. Baroody, 8410
C. S. Selvage, 8420
C. M. Tapp, 8460
R. C. Wayne, 8450
P. J. Eicker, 8451
A. C. Skinrood, 8452
W. G. Wilson, 8453
R. W. Carling, 8453 (15)
L. G. Radosevich, 8453
Publications Division, 8265, for TIC (2)
Publications Division, 8265/Technical Library Processes and Systems Division, 3141
Technical Library Processes and Systems Division, 3141 (2)
M. A. Pound, 8214, for Central Technical Files (3)